A Wide Range and High Conversion Gain Power Detector for Frequency Shift Sensing Applications

Chua-Chin Wang†, *Senior Member, IEEE*, Deng-Shian Wang, Shiou-Ya Chen, and Chia-Ming Chang
Department of Electrical Engineering, National Sun Yat-Sen University, Kaohsiung, Taiwan 80424
Email: ccwang@ee.nsysu.edu.tw

***Abstract*—This paper demonstrates a high frequency power detector with high conversion gain for frequency-shift sensing applications used in biosensing systems. The proposed design comprises an amplitude-to-voltage convertor (AVC), a peak detector, and a bandgap. To increase the operating frequency range, AVC utilizes half of an RMS power detector to attain the power measure of an input signal. Since the input power is converted to a DC voltage by AVC, the peak detector will secure the resonant frequency when AVC generates the highest voltage. The proposed power detector circuit is realized on silicon using a 60 V 0.25 μm CMOS technology. Measurement results show that the proposed circuit is able to detect input frequency from 500 Hz to 2.5 GHz. The conversion gain of AVC is 166.6 mV/dB, and the power consumption is 5.25 mW given a 5 V power supply voltage.**

***Index Terms*—Analog processing circuit, resonant frequency, power detector, peak detector, frequency-shift readout circuit**

I. Introduction

Recently, MEMS sensors with resonant features have been widely used in many applications, e.g., antigen concentration sensing [1], CO_2 concentration sensing [2], and temperature sensing [3], etc., where frequency detectors for sensors are needed. Fig. 1 shows a typical frequency detector circuit. The control circuit generators a frequency-scanning signal to the sensor. When the frequency of the frequency-scanning signal equals to the sensor's resonant frequency, the maximum or minimum power will be presented. The power detector then generates a digital signal to the control circuit to lock the detected frequency. However, different types of sensors are featured with different frequency ranges. For example, the FPW (flexural plate wave) devices able to estimate IgE (immunoglobulin E) antigen concentration are found to work in the range from 2 MHz to 10 MHz [1]. The SAW (surface acoustic resonator) able to sense the CO_2 concentration must be operated around 545 MHz [2]. The FBAR (film bulk acoustic resonator) for the temperature sensing works around 2.19 GHz [3]. Therefore, to accommodate the operating frequency ranges of various sensors, a wide input range power detector is needed.

The power detectors in previous works can be categorized into two types by the input frequency range. The first type employs a peak voltage detector to be the power detector [4]. Since the peak detector includes OPA or OTA, it is limited in the low frequency range. The other type is RMS power detector, as shown in Fig. 2 [5]. Although RMS power detectors can operate in a high frequency range, but it has the offset error problem and the output voltage resolution, V_{diff}, is too small [6]. In order to increase the output difference, an amplifier following the RMS power detector is usually added to enlarge the output voltage. Unfortunately, the offset error will be amplified as well. Therefore, the operating frequency range of the RMS power detector is limited by the offset error.

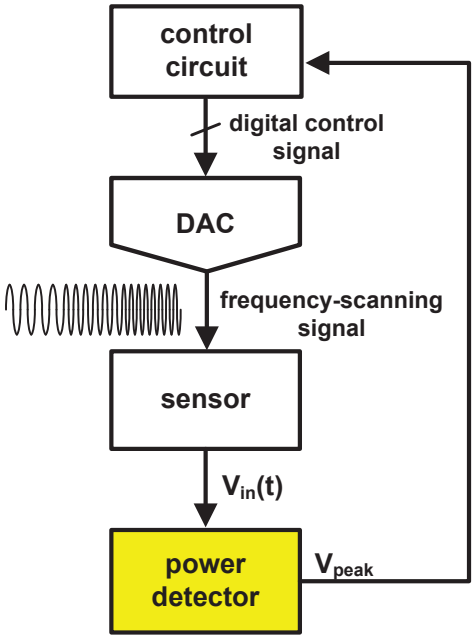

Fig. 1. Architecture of a typical frequency-shift detection circuit

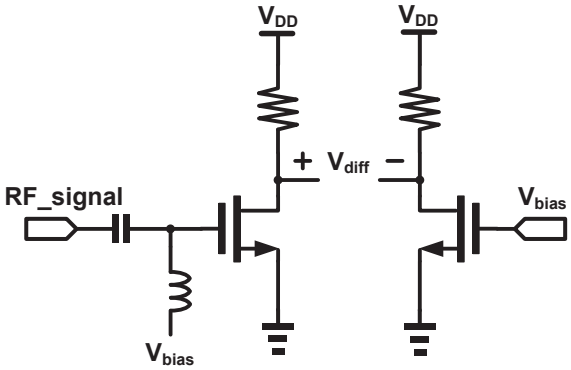

Fig. 2. Schematic of the RMS power detector [5]

In this paper, a wide input frequency range power detector has been presented. To cancel the offset error and increase the

input frequency, we propose to use half of RMS power detector to convert the input amplitude into a DC voltage, namely amplitude-to-voltage convertor (AVC). Following the AVC, the peak detector is available to detect the resonant frequency.

II. Power Detector in a Sensing System

Fig. 3 shows the architecture of the proposed power detector. $V_{in}(t)$ is a time-domain voltage signal generated by a sensor. The proposed power detector converts the $V_{in}(t)$ into a peak voltage, $\mathrm{V_{peak}}$, which is sent to the following μC-based DSP core to be analyzed and processed. Besides, μC-based DSP core is also used to control the DAC to generate the frequency-scanning signal. The power detector consists of an AVC, a peak detector, and a bandgap. Notably, this architecture is meant for the applications which the frequency response of the biosensor is a band-reject filter. If the frequency response is a band-pass filter, the peak detector should be replaced with a valley detector.

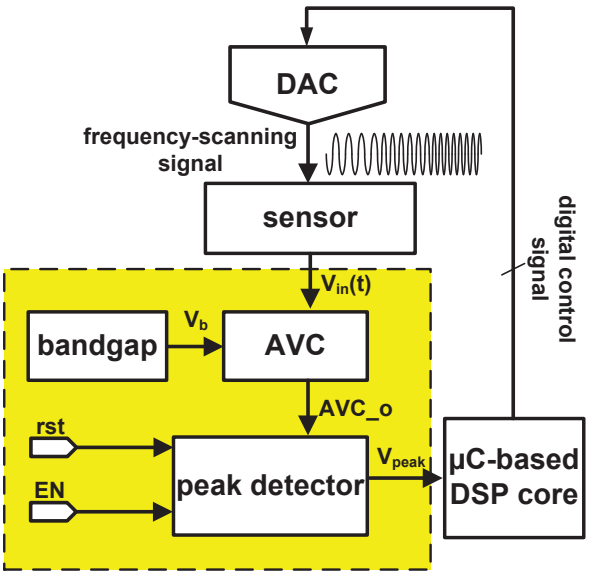

Fig. 3. System view using the proposed power detector

III. Circuit Design and Analysis

A. Amplitude-to-voltage convertor (AVC)

To cancel the offset error, AVC, shown in Fig. 4, is carried out by only half of the RMS power detector circuit. $\mathrm{C_{201}}$ is utilized to decouple the DC term of $V_{in}(t)$, where $V_{in}(t)$ is the output signal from the sensor. V_b is a stable DC bias driving $\mathrm{M_{201}}$ into the saturation region. Thus, the drain current of $\mathrm{M_{201}}$ can be expressed as follow.

$$i_{M_{201}}(t) = \frac{1}{2} \cdot \beta_n \cdot \left(V_{in}(t) + V_b - V_{TN}\right)^2 \quad (1)$$

where $\beta_n = \mu_n C_{ox}\,(W_{201}/L_{201})$ is the MOSFET transconductance parameter, μ_n is the electron mobility, C_{ox} is the gate oxide capacitance per unit area, V_{TN} is the NMOS threshold voltage, W_{201} and L_{201} are the channel width and length of $\mathrm{M_{201}}$, respectively. $\mathrm{M_{202}}$ is biased in the triode region to act as a resistor. The resistance can be written as follows.

$$r_{M_{202}} = 1/\beta_p \cdot \left(V_{DD} - |V_{TP}|\right) \quad (2)$$

where $\beta_p = \mu_p C_{ox}\,(W_{202}/L_{202})$, μ_p is the hole mobility, V_{TP} is the PMOS threshold voltage. W_{202} and L_{202} are the channel width and length of $\mathrm{M_{202}}$, respectively. $\mathrm{C_p}$ is a low-pass filter to filter out the AC component of AVC_o. When the current $i_{M_{201}}(t)$ flowing through the resistor $r_{M_{202}}$ and $V_{in}(t)$ is substituted with $V_a \cdot \cos(2\pi \mathrm{ft} + \theta)$, the DC term of the output voltage is attained as follows.

$$AVC\_o = V_{DD} - \frac{1}{2} \cdot \beta_n \cdot r_{M_{202}} \cdot \left[V_a^2 + \left(V_b - V_{TN}\right)^2\right] \quad (3)$$

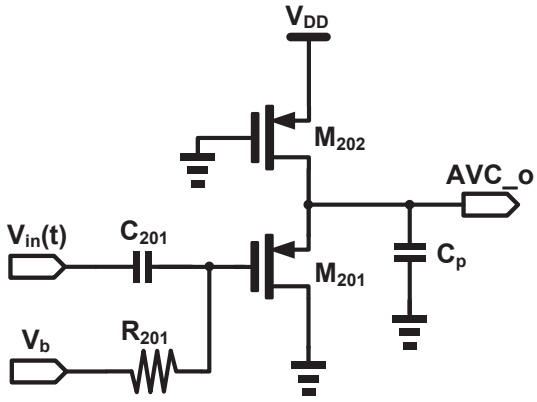

Fig. 4. Schematic of AVC

Fig. 5 shows the simulation result of AVC output voltage vs. the input amplitude, while Fig. 6 is that of AVC output vs. the input frequency. These two figures demonstrate that the output voltage is irrelevant with the input frequency. However, AVC output voltage increases as the input amplitude decreases. Therefore, when the frequency-scanning signal is equal to the resonant frequency of the sensor, which the frequency response acts like a band-reject filter, the minimum output amplitude will be found, and AVC generates the highest output voltage.

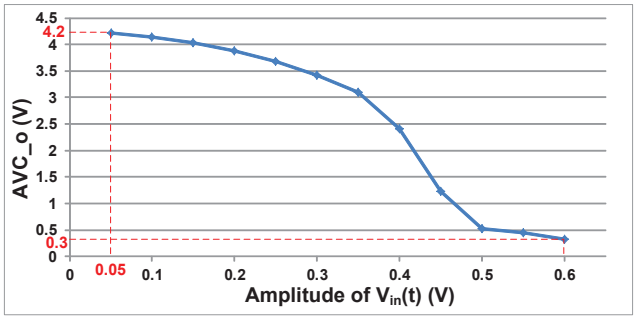

Fig. 5. Simulation result of AVC output voltage vs. the input amplitude

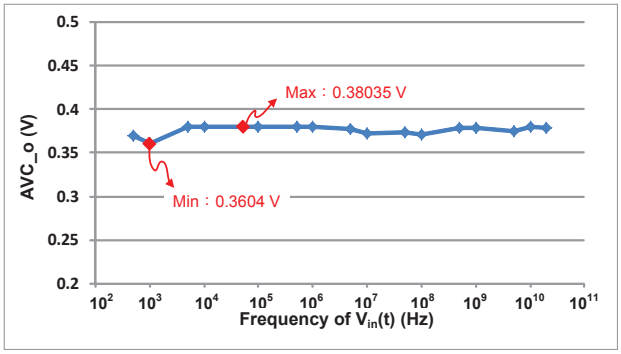

Fig. 6. Simulation result of AVC output voltage vs. the input frequency

B. Peak detector

To reduce the power consumption, the proposed peak detector composed by an OPA which can be turned off when EN is high, as shown in Fig. 7. When the frequency of the frequency-scanning signal increases over the resonant frequency, the output of the peak detector, V_{peak}, stores the last highest voltage.

By the simulation result shown in Fig. 5, the conversion gain of AVC is 176 mV/dB, and the sensitivity of the peak detector is simulated to be 10 mV. Therefore, the sensitivity of the entire power detector is 0.06 dB. According to the frequency response of the sensors [7]-[9], the proposed power detector can detect the resonant frequency with less than 10% error given such a 0.06 dB sensitivity.

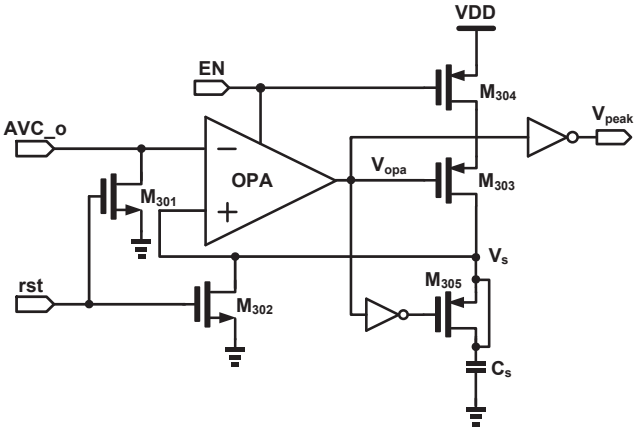

Fig. 7. Schematic of the peak detector

IV. Implementation and Measurement

The proposed power detector is realized using TSMC 60V 0.25 μm CMOS technology. Fig. 8 shows the die photo of the proposed power detector. The area is $685 \times 615\ \mu m^2$.

Fig. 9 shows the measurement environment of proposed power detector. ABM PRT3230 generates supply voltage, Tektronix AFG3252 generates EN and rst signal (low frequency), and KEYSIGHT N5171B generates $V_{in}(t)$. Then, LeCroy 610Zi is used to observe the signals. Fig. 10 and Fig. 11 show the measurement results of the proposed power detector. Fig. 10 shows the input $V_{in}(t)$ and output (AVC_o) of AVC. $V_{in}(t)$ is an AM (amplitude modulation) signal and the frequency of the carrier wave is 2.5 GHz. As previously mentioned, the higher the amplitude of $V_{in}(t)$ is, the lower the voltage of AVC_o will be, then peak detector is used to detect the highest voltage of AVC_o, as shown in Fig. 11. To reduce power consumption, EN is used to enable (EN=0) or disable the OPA in the peak detector, where the peak detector is operated in sample and hold state, respectively. Fig. 11 (a) shows the measurement results of the peak detector in five consecutive actions. Fig. 11 (b) shows the same scenario but the OPA is always turned on. Most importantly, the power consumption is reduced by 23% when the frequency of the EN is as high as 15 kHz.

The comparison with several prior works is tabulated in Table I. The proposed design attains the second widest frequency range, 500 Hz to 2.5 GHz, and the second highest conversion gain of AVC, 166.6 mV/dB.

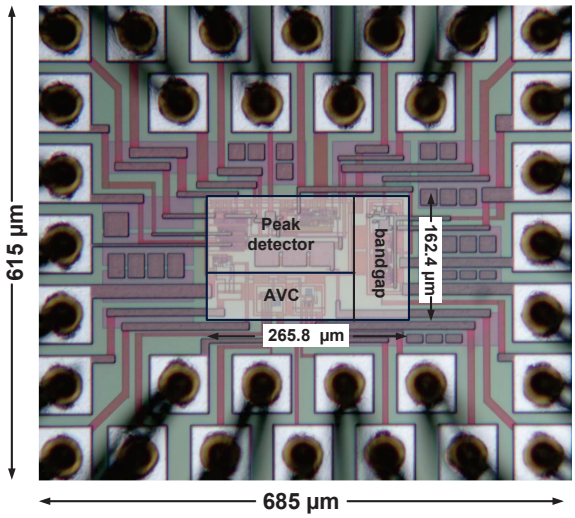

Fig. 8. The chip photo of proposed design

V. Conclusion

This paper presents a wide input frequency range power detector for frequency-shift applications. The proposed circuit is able to detect the input frequency from 500 Hz to 2.5 GHz. By the measurement results, the conversion gain of AVC is 166.6 mV/dB and the power consumption of the entire circuit is reduced 23% provided that the switching frequency of the enable is 15 kHz.

Acknowledgement

This investigation is partially supported by Ministry of Science and Technology under grant NSC 102-2221-E-110-081-MY3. The authors would like to express their deepest gratefulness to Chip Implementation Center of National Applied Research Laboratories, Taiwan, for their thoughtful chip fabrication service and EDA tool support.

TABLE I
COMPARISON WITH PRIOR WORKS

	[6]	[10]	[11]	[5]	[12]	this work*
Year	2008	2008	2009	2012	2014	2015
Process	0.13 μm CMOS	0.35 μm CMOS	0.35 μm CMOS	0.18 μm CMOS	0.25 μm CMOS	0.25 μm CMOS
Conversion Gain (mV/dB)	6	50	6	17	176	166.6
Supply voltage	1.2 V	3.3 V	3.3 V	1.8 V	5 V	5 V
Frequency range	0.125 GHz ~8.5 GHz	0.9 GHz ~2.4 GHz	3.1 GHz ~10.6 GHz	0.5 GHz ~5 GHz	500 Hz ~20 GHz	500 Hz ~2.5 GHz
Power Consumption (mW)	0.18 (RMS power detector)	N/A	N/A	0.9 (RMS power detector)	1.96 (power detector)	5.25 (full circuit)

* measurement results

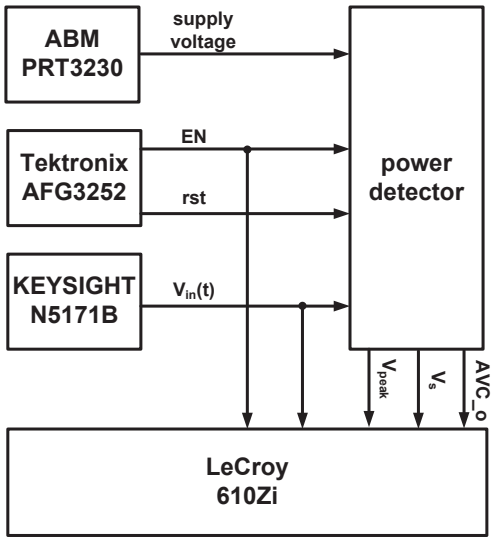

Fig. 9. Measurement environment

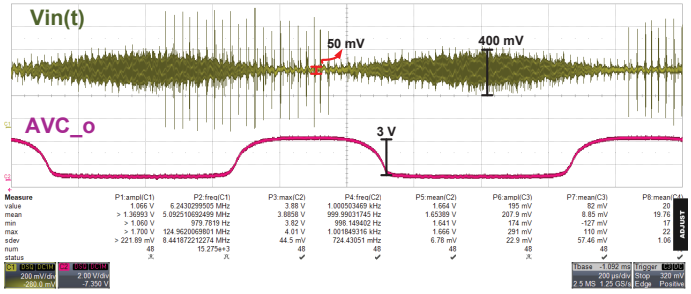

Fig. 10. The measurement result of AVC

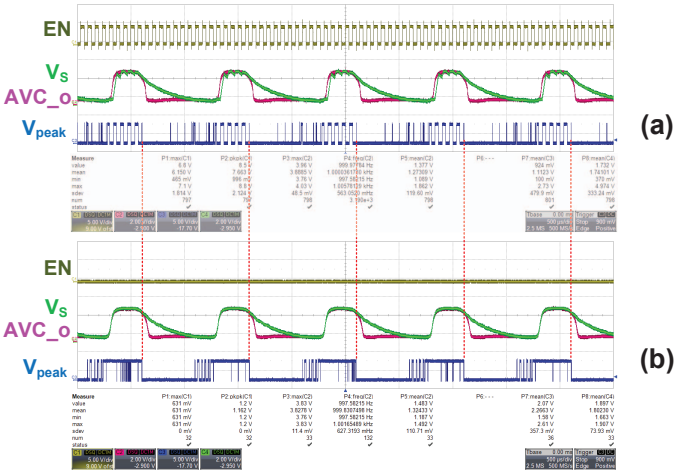

Fig. 11. The measurement result of the peak detector. (a) EN is a periodic signal (b) EN is a DC 0 V signal

REFERENCES

[1] C.-H. Hsu, Y.-R. Lin, Y.-D. Tsai, Y.-C. Chen, and C.-C. Wang, "A frequency-shift readout system for FPW allergy biosensor," *IEEE Inter. Conf. on IC Design & Technology (ICICDT),* pp. 1-4, May 2011.

[2] S. Fanget, H. Grange, F. Palancade, G. Ganuchaud, M. Matheron, S. Charlot, T. Bordy, T. Hoang, P. Rey, D. Mercier, P. Brunet-Manquat, and P. Robert, "CO2 measurement using an AlN/SI SAW sensor," *IEEE Inter. Conf. on Solid-State Sensors, Actuators and Microsystems,* pp. 1136-1139, Jun. 2011.

[3] Z. Wang, X. Qiu, J. Oiler, J. Zhu, and R. Hu, "Film bulk acoustic-wave resonator (FBAR) based infrared sensor," *IEEE Inter. Conf. on Nano/Micro Engineered and Molecular Systems (NEMS),* pp. 824-827, Jan. 2010.

[4] B. Rumberg and D. W. Graham, "A low-power magnitude detector for analysis of transient-rich signals," *IEEE Journal of Solid-State Circuits,* vol. 47, no. 3, pp. 676-685, Mar. 2012.

[5] S. Sakphrom and A. Tranachayanont, "A low-power CMOS RF power detector," *IEEE Inter. Conf. on Electronics, Circuits and Systems (ICECS),* pp. 177-180, Dec. 2012.

[6] Y. Zhou and Y.-W Chia, "A low-power ultra-wideband CMOS true RMS power detector," *IEEE Tran. on Microwave Theory and Techniques,* vol. 56, no. 5, pp. 1052-1058, May 2008.

[7] T. Yokoyama, T. Nishihara, S. Taniguchi, M. Iwaki, Y. Satoh, M. Ueda, and T. Miyashita, "New electrode material for low-loss and high-Q FBAR filters," *IEEE Inter. on Ultrasonics Symposium,* vol. 1, pp. 429-432, Aug. 2004.

[8] S. H. Yoon and D.-J. Kim, "Fabrication and characterization of ZnO films for biological sensor application of FPW device," *IEEE Inter. Symposium on Applications of Ferroelectrics,* pp. 1-4, Aug. 2006.

[9] S. Fujii and C. Jian, "High-frequency SAW filters based on diamond films," *IEEE Tran. on Ultrasonics, Ferroelectrics and Frequency Control,* vol. 59, no. 12, pp. 2758-2764, Dec. 2012.

[10] A. Valdes-Garcia, R. Venkatasubramanian, J. Silva-Martinez, and E. Sanchez-Sinencio, "A broadband CMOS amplitude detector for on-chip RF measurements," *IEEE Tran. on Instrumentation and Measurement,* vol. 57, no. 7, pp. 1470-1477, Jul. 2008.

[11] K. A. Townsend and J. W. Haslett, "A wideband power detection system optimized for the UWB spectrum," *IEEE Journal of Solid-State Circuits,* vol. 44, no. 2, pp. 371-381, Feb. 2009.

[12] C.-C. Wnag, D.-S. Wnag, S.-Y. Chen, and C.-M. Chang, "A 20 GHz power detector with 176 mV/dB conversion gain," *2014 IEEE Pacific Conf. on Circuits and Systems (APCCAS),* pp. 17-20, Nov. 2014 .